Original Article

Induction of *MYCN*-amplified neuroblastoma differentiation through NMYC suppression using PPAR-γ antagonist

Yukako Nakao-Ise,[1] Takumi Narita,[1] Shingo Miyamoto,[1] Motoki Watanabe,[1] Takuji Tanaka,[2] Yoshihiro Sowa,[1] Yosuke Iizumi,[1] Mitsuharu Masuda,[1] Gen Fujii,[3] Yasuko Hirai,[4] Toshimasa Nakao,[1,5] Hideki Takakura,[1,6] and Michihiro Mutoh[1,*]

[1]Department of Molecular-Targeting Prevention and [4]Department of Human Immunology and Nutrition Science, Kyoto Prefectural University of Medicine, Kawaramachi-Hirokoji, Kamigyo-ku, Kyoto 602-8566, Japan
[2]Department of Diagnostic Pathology & Research Center of Diagnostic Pathology, Gifu Municipal Hospital, 7-1 Kashima-cho, Gifu 500-8513, Japan
[3]Central Radioisotope Division, National Cancer Center Research Institute, 5-1-1 Tsukiji, Chuo-ku, Tokyo 104-0045, Japan
[5]Organ Transplantation Center, National Center for Child Health and Development, 2-10-1 Okura, Setagaya-ku, Tokyo 157-8535, Japan
[6]Laboratory of Biopharmaceutics and Pharmacokinetics, Faculty of Pharmaceutical Sciences, Hiroshima International University, 5-1-1 Hirokoshingai, Kure city, Hiroshima 737-0112, Japan

(Received 27 April, 2023; Accepted 21 June, 2023; Released online in J-STAGE as advance publication 28 June, 2023)

Neuroblastomas are the most common extracranial solid tumors in children and have a unique feature of neuronal differentiation. Peroxisome proliferator-activated receptor (PPAR)-γ is reported to have neuroprotective effects in addition to having antitumor effects in various cancers. Thus, we aimed to clarify the role of PPAR-γ agonist and antagonist in malignant neuroblastomas, which also possess neuronal features. In *MYCN*-amplified neuroblastoma CHP212 cells, treatment with the PPAR-γ antagonist GW9662 induced growth inhibition in a dose-dependent manner. In addition, the PPAR-γ antagonist treatment changed cell morphology with increasing expression of the neuronal differentiation marker tubulin beta 3 (TUBB3) and induced G1 phase arrest and apoptosis in *MYCN*-amplified neuroblastoma. Notably, the PPAR-γ antagonist treatment significantly decreased expression of NMYC, B-cell lymphoma 2 (BCL2) and bromodomain-containing protein 4 (BRD4). It is implied that BRD4, NMYC, BCL2 suppression by the PPAR-γ antagonist resulted in cell growth inhibition, differentiation, and apoptosis induction. In our *in vivo* study, the PPAR-γ antagonist treatment induced CHP212 cells differentiation and resultant tumor growth inhibition. Our results provide a deeper understanding of the mechanisms of tumor cell differentiation and suggest that PPAR-γ antagonist is a new therapeutic and prevention option for neuroblastomas.

***Key Words*: neuroblastoma, PPAR-γ, NMYC, BCL2, BRD4**

Neuroblastoma is the most common extracranial solid tumor in children. This embryonal tumor, derived from the neural crest tissue, arises in the sympathetic nervous system.(1) Neuroblastoma has a higher frequency of spontaneous regression than other tumors in infancy, and this is its unique feature.(2) Patients with low- and intermediate-risk neuroblastoma have good 5-year survival rates of >95% and >90%, respectively.(3) Amplification of the *MYCN* oncogene is closely correlated with advanced stages of the disease and poor survival. However, about 20–30% of patients with neuroblastoma show *MYCN* amplification, which is a cause of concern.(3,4) Despite recent chemotherapy advances, 5-year survival rates of high-risk groups, including patients with *MYCN* amplification, have shown only modest improvement (approximately 40–50%).(1) Moreover, 50–60% of patients with high-risk neuroblastoma are said to be relapsed after completing treatment.(5) Therefore, novel treatment options whose purpose are not only remission but also recurrence inhibition are required for children with high-risk neuroblastoma. We believe that induction of differentiation in neuroblastomas, which might be related to tumor progression and regression, including spontaneous regression, could be a strong therapeutic strategy for remission and inhibition of recurrence.(6)

Peroxisome proliferator-activated receptor (PPAR)-γ, a ligand-dependent transcription factor of the nuclear hormone receptor, has various effects on neuronal proliferation, differentiation, and apoptosis during neuronal maturation.(7–9) Treatment with PPAR-γ agonists is reported to prevent neuronal cell death and apoptosis in ischemic stroke, status epilepticus, and degenerative disorders such as Alzheimer's, Parkinson's, and Huntington's disease.(10–12) In addition to having anti-neuronal apoptotic effects, PPAR-γ agonists are known to induce apoptosis in various cancer cells, including breast, thyroid, colon, and lung cancer cells.(13–15)

PPAR-γ has contradictory effects in neuroblastoma. For example, relatively high concentrations of PPAR-γ agonists for *MYCN*-amplified and -non-amplified neuroblastoma/high concentrations of antagonists for *MYCN*-non-amplified neuroblastoma have been reported to exert antitumor effects.(16,17) Therefore, the role of PPAR-γ in neuroblastoma, which is a malignant tumor that also has neuronal features typified by neuronal differentiation, remains unclear. Thus, we aimed to clarify the effects of PPAR-γ agonists and antagonists on *MYCN*-amplified and -non-amplified neuroblastoma.

In the present study, we demonstrate that treatment with a PPAR-γ antagonist significantly induces the differentiation and inhibits the growth of *MYCN*-amplified neuroblastoma. Furthermore, we demonstrate the underlying mechanisms and confirm its differentiation in an *in vivo* subcutaneous tumor model.

Materials and Methods

Chemicals. GW9662 was obtained from Sigma-Aldrich (M6191; St. Louis, MO). GW9662 is a selective PPAR-γ antagonist that inhibits adipogenesis of primary preadipocytes. Rosiglitazone was obtained from Calbiochem (557366; San Diego, CA). Rosiglitazone is a pure PPAR-γ agonist and is used

*To whom correspondence should be addressed.
E-mail: mimutoh@koto.kpu-m.ac.jp

doi: 10.3164/jcbn.23-28

as a blood-glucose-lowering drug and a potent thiazolidinedione insulin sensitizer. 13-cis-retinoic acid (RA) was obtained from Tokyo Chemical Industry Co., Ltd. (R0088; Tokyo, Japan).

Cell culture. The human neuroblastoma cell lines CHP212 (CRL-2273, RPID: CVCL_1125), SK-N-AS (CRL-2137, RPID: CVCL_1700), and BE(2)C (CRL-2268, RPID: CVCL_007) were obtained from American Type Culture Collection (Manassas, VA), and IMR32 (JCRB9050, RPID: CVCL_0346) cells were obtained from Japanese Collection of Research Bioresources Cell Bank (Osaka, Japan). The cells were cultured in RPMI 1640 medium supplemented with 5% heat-inactivated fetal bovine serum and antibiotics (100 µg/ml streptomycin and 100 U/ml penicillin) at 37°C in 5% CO_2. For *MYCN* amplification or non-amplification, cells were selected from a previous study.[18]

Cell growth assay (colony formation assay). Cells were seeded in six-well plates and incubated overnight. After treatment, the cells were further incubated for 9 days. The culture medium was not replaced. At endpoint, cells were fixed with 4% formaldehyde and stained with 0.1% crystal violet. After staining, the area of the stained colonies was calculated using the ImageJ software (all cells in the plate were evaluated; the value for untreated control cells was set to 1).

Cell cycle assay. CHP212 cells were seeded in six-well plates and incubated overnight and then treated with GW9662. Six days later, the cells were trypsinized, fixed with 70% ethanol, and stored at −20°C overnight. The cells were then processed using Tali™ Cell Cycle Kit (A10796; Invitrogen, Waltham, MA) and incubated at room temperature in the dark for 30 min. Analyses were performed using Tali™ Image-based Cytometer (Invitrogen).

Apoptosis assay (Annexin V assay). CHP212 cells were seeded in 24-well plates, incubated overnight, and then treated with GW9662. Seven days later, the cells were stained using Tali™ Apoptosis Kit (A10788; Invitrogen) and analyzed using Tali™ Image-based Cytometer.

Immunocytochemical staining. CHP212 cells were seeded and incubated overnight and then treated with GW9662 or 13-cis-RA in a 12-well plate. Seven days later, the cells were fixed with 4% paraformaldehyde and permeabilized with 0.2% Triton X-100 in PBS at room temperature for 10 min. Protein block buffer was applied to the cells (ab64226; Abcam, Cambridge, UK); they were then incubated for 1 h and stained with a primary antibody against tubulin beta 3 (TUBB3) (801213; Biolegend, San Diego, CA) and MAP2 (ab32454; Abcam) in PBS solution containing 1% bovine serum albumin (BSA) and 0.05% Triton X-100 overnight at 4°C. The cells were then incubated with Alexa Fluor® 488 goat anti-mouse IgG (50126A; Invitrogen) for 1 h at room temperature, followed by nuclear counterstaining with Hoechst 33342 (346-07951; DOJINDO, Kumamoto, Japan). Images were captured using a 40× objective. The circularity {4π/[area x (circumference)2]} of all cells was calculated using software, ImageJ.

Western blot analysis. CHP212 cells were seeded in 6-well plate and incubated overnight and then treated with GW9662. After indicated days, cells were lysed with sample buffer (pH 6.8 0.5 M Tris-HCl 1 ml, 10% SDS 2 ml, β-mercaptoethanol 0.6 ml, glycerol 1 ml, distilled water 5.4 ml, several drops of 1% BPB). Western blot was performed according to standard protocol. Cell lysates were electrophoresed on Mini-PROTEAN TGX Stain-Free gels (Bio-Rad Laboratories, Hercules, CA) and transferred to PVDF membranes. Then, the membranes were incubated with primary antibodies followed by the corresponding secondary antibodies. NMYC mouse monoclonal (sc-53993; Santa Cruz Biotechnology, Dallas, TX), B-cell lymphoma 2 (BCL2) rabbit monoclonal (ab32124; Abcam), bromodomain-containing protein 4 (BRD4) mouse monoclonal (sc-518021; Santa Cruz Biotechnology), TUBB3 (801213; Biolegend), Neurofilament-L (NFL, 2837; Cell Signaling Technology, Beverly, MA), NeuroD1 (ab60704; Abcam), and β-actin mouse monoclonal (A5441; Sigma-Aldrich) antibodies were the primary antibodies used. NMYC and BRD4 antibodies were applied at a 1:200 dilution, TUBB3 antibody at 1:500, BCL2, NFL and NeuroD1 antibodies at 1:1,000, and β-actin antibody at 1:2,000. Peroxidase-conjugated anti-rabbit and anti-mouse IgG secondary antibodies (NA934V, NA931V; GE Healthcare, Little Chalfont, UK) were also used. Blots were developed using Immobilon™ Western

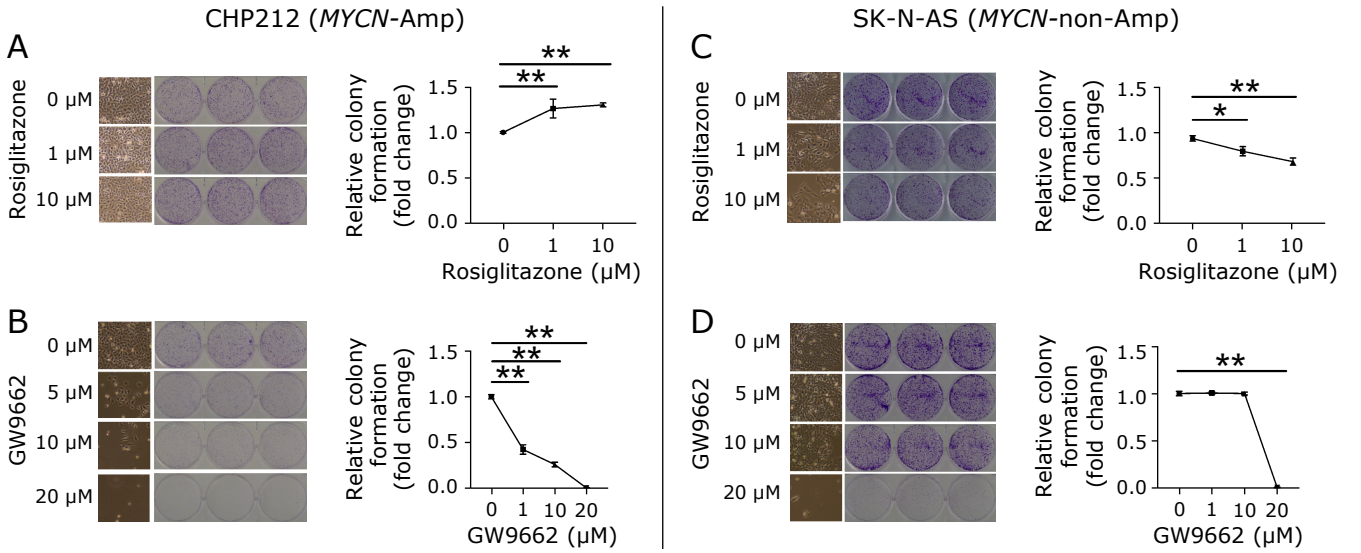

Fig. 1. Change in cell growth after treatment with the PPAR-γ agonist rosiglitazone and the PPAR-γ antagonist GW9662. Cells were seeded in six-well plates at a density of 1 × 10^4 cells/well. After overnight incubation, the cells were treated with the indicated doses of rosiglitazone or GW9662 for 9 days. At the end of the experiment, microphotographs (×10) were obtained using a phase-contrast microscope (left row). The cells were further stained with crystal violet and imaged (middle row). Moreover, the area of the stained colonies was quantified using ImageJ (right row). (A) CHP212 cells were treated with rosiglitazone or untreated. (B) CHP212 cells were treated with GW9662 or untreated; (C) SK-N-AS cells were treated with rosiglitazone or untreated. (D) SK-N-AS cells were treated with GW9662 or untreated. Data are presented as the mean ± SE (n = 3). *p<0.05; **p<0.01, relative to non-treated control. P values were calculated using Tukey's multiple comparison test. The scales of horizontal axes in (A)–(D) are linear scale.

doi: 10.3164/jcbn.23-28

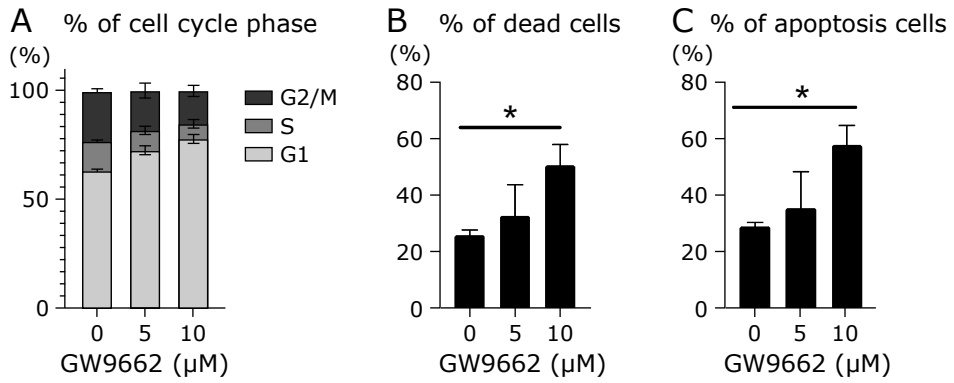

Fig. 2. Effect of GW9662 treatment on cycle distribution and apoptosis in CHP212 cells. CHP212 cells were seeded in six-well plates at a density of 8×10^4 cells/well, incubated overnight, and then treated with the indicated doses of GW9662 for 6 days. At the end of the experiment, the distribution of cells in the G1, S, and G2/M phases was analyzed using Tali™ Image-based Cytometer, as shown in (A). CHP212 cells were seeded in 24-well plates at a density of 1×10^4 cells/well and treated with the indicated doses of GW9662 for 7 days. (B) Dead cells (PI-positive cells) and (C) apoptotic cells (annexin V-positive cells) were evaluated using Tali™ Image-based Cytometer. Data are presented as the mean ± SE ($n = 3$). *$p<0.05$, relative to untreated control. *P* values were calculated using Tukey's multiple comparison test.

Chemiluminescent HRP Substrate (Millipore Corporation, Billerica, MA) and scanned using ASHERSHAM Image Quant 800 (Cytiva, Marlborough, MA).

Adherent cell assay. Cells treated with or without 10 μM GW9662 were seeded in 24-well plates. After 5 h, the cells were fixed with 4% paraformaldehyde and stained with 0.2% Coomassie Brilliant Blue G-250 in water containing 10% acetic acid and 40% methanol. After they were completely dried, 0.1 N NaOH in 50% methanol and the same quantity of 10% trichloroacetic acid were added. The absorbance at 596 nm wavelength was measured using Thermo Scientific™ Multiskan™ FC (Thermo Fisher Scientific, Waltham, MA). For 100% attached wells, cells were seeded in 24-well plates coated with poly-L-lysine (0403; ScienCell, Carlsbad, CA) at the dish bottom. For 0% attached wells, no coating was used, and no cells were seeded in the well.

***In vivo* xenograft assay.** Four-week-old female nude mice (BALB/cAJcl-nu/nu) were purchased from CLEA Japan Inc. (Tokyo, Japan). A total of 5×10^6 human *MYCN*-amplified neuroblastoma CHP212 cells, or 1.75×10^6 human *MYCN*-non-amplified neuroblastoma SK-N-AS cells, were each mixed with matrix gel, Geltrex™ (A14132-02; Gibco, Thermo Fisher Science), including vehicle (0.2% DMSO) or PPARγ antagonist (10 μM GW9662), and injected subcutaneously into the back of each mouse. Tumor diameters were measured once a week using calipers, and tumor volumes were calculated according to the following formula: tumor volume (mm^3) = $1/2 \times A \times B^2$ (A = largest diameter, B = smallest diameter). The mice were humanely sacrificed after 4–5 weeks, and tumors were harvested. The harvested tumors were measured using the following formula: tumor volume (mm^3) = $A \times B \times C \times \pi/6$ (A = largest diameter, B = smallest diameter, C = height).

Tumor histological analysis. The tumor tissues removed were fixed with 4% paraformaldehyde. After being embedded in paraffin, the tissue sections were prepared and stained with hematoxylin and eosin (H & E) (Kyoto Microbio Laboratory, Kyoto, Japan).

Statistical analysis. Data are presented as the mean ± SE of three experiments. Statistical analyses were performed using GraphPad Prism (ver. 8.4.3; GraphPad Software Inc, San Diego, CA). The two different groups were analyzed using an unpaired *t* test. Differences among groups were evaluated using one-way analysis of variance (ANOVA). *In vivo* tumor volume graphs were analyzed using two-way ANOVA. Multiple comparisons were performed using Tukey's multiple comparison test relative to the untreated control. Statistical significance was set at $p<0.05$.

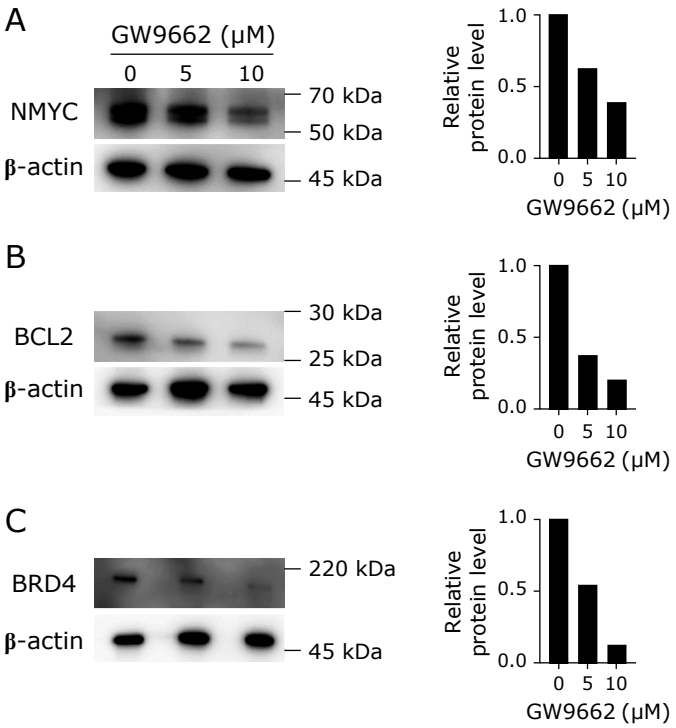

Fig. 3. Protein expression changes in NMYC, BCL2, and BRD4 by GW9662 treatment. CHP212 cells were seeded in six-well plates at a density of 8×10^4 cells/well, incubated overnight, and treated with the indicated dose of GW9662 for 5 days. NMYC (A), BCL2 (B), and BRD4 (C) were detected using western blot analysis. β-actin was used as the internal control. The data are representative of data from two independent experiments.

Results

PPAR-γ antagonist GW9662 treatment induces growth inhibition in *MYCN*-amplified neuroblastoma cells. To clarify the effects of treatment with PPAR-γ agonist and antagonist on the growth of neuroblastoma cells, we performed colony formation assay after a 9-day treatment with either 0, 1, and 10 μM rosiglitazone (PPAR-γ agonist) or 0, 5, 10, 20 μM GW9662 (PPAR-γ antagonist). In the case of *MYCN*-amplified neuroblastoma CHP212 cells, cell growth was increased by

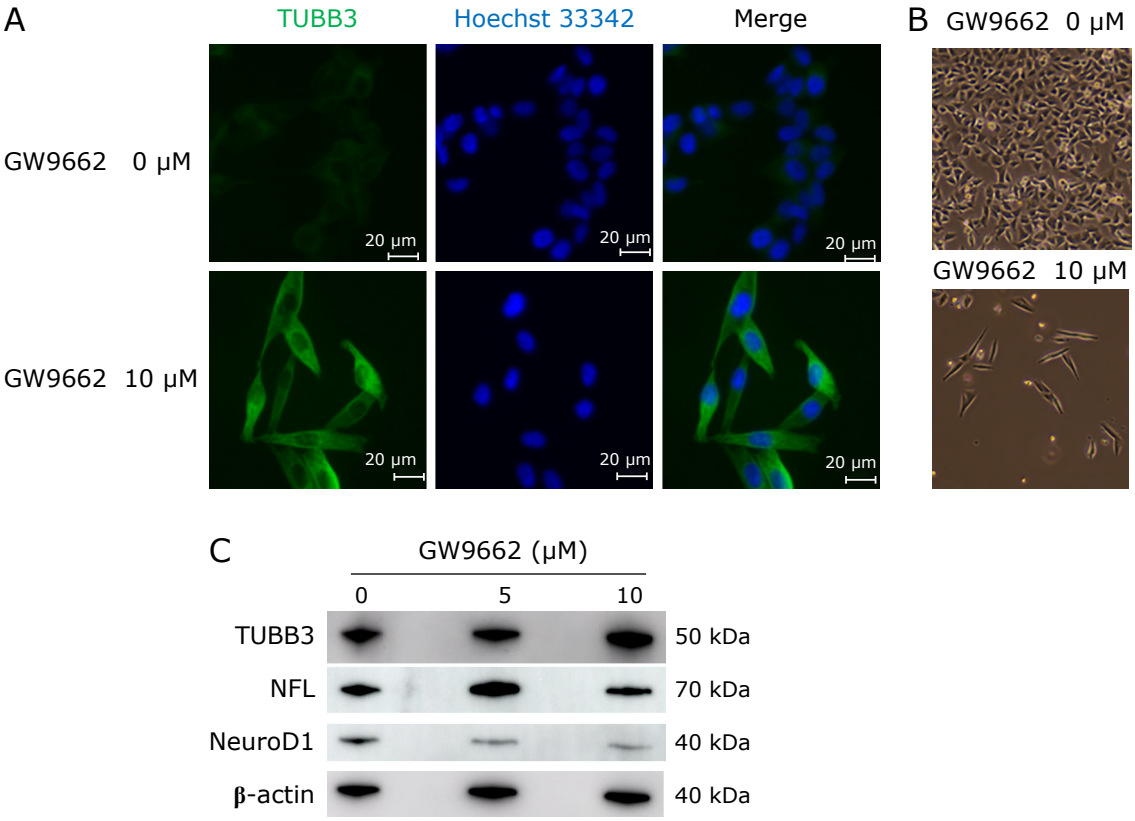

Fig. 4. Upregulation of the neuronal marker TUBB3 by GW9662 treatment. (A) CHP212 cells were seeded in 12-well plates at a density of 5×10^3 cell/well, incubated overnight, and then exposed to 0 μM or 10 μM GW9662. Seven days after the treatment with GW9662, the cells were stained with an antibody directed against TUBB3 (green), and nuclei were stained with Hoechst 33342 (blue). The cells were examined using fluorescence microscopy (×40, bar: 20 μm). At the end of the experiment day, before immunostaining, microphotographs (×10) were taken using phase-contrast microscopy (B). (C) CHP212 cells were seeded in six-well plates at a density of 8×10^4 cells/well, incubated overnight, and treated with the indicated dose of GW9662 for 7 days. TUBB3, NFL, NeuroD1 were detected using western blot analysis. β-actin was loaded as an internal control. See color figure in the on-line version.

treatment with low-to-moderate doses of rosiglitazone, whereas it was decreased by GW9662 treatment in a dose-dependent manner (Fig. 1A and B). Cell growth inhibition by GW9662 treatment was also observed in the other *MYCN*-amplified neuroblastoma cells [BE(2)C and IMR32] (Supplemental Fig. 1A and B*). In contrast, in the case of *MYCN*-non-amplified neuroblastoma SK-N-AS cells, cell growth was decreased by rosiglitazone treatment and were not changed clearly excepting high concentration of GW9662 (Fig. 1C and D). Furthermore, remarkable morphological changes were observed in CHP212 cells treated with GW9662 at concentrations >10 μM (Fig. 1B). Treatment with 20 μM GW9662 resulted in almost complete cell detachment (Fig. 1B and D).

GW9662 treatment induces G1 phase arrest and apoptosis in *MYCN*-amplified neuroblastoma CHP212 cells. To further examine the growth inhibitory effect of PPAR-γ antagonist on *MYCN*-amplified neuroblastoma, we performed cell cycle and apoptosis assays. CHP212 cells treated with 5 and 10 μM GW9662 showed increases in the number of G1 phase cells and decreases in the number of S phase cells. This indicates that G1 arrest was induced by GW9662 treatment (Fig. 2A). Moreover, increased numbers of dead and apoptotic cells were observed, and the data indicated that the proportion of dead cells was almost the same as that of apoptotic cells (Fig. 2B and C).

GW9662 treatment inhibits NMYC, BCL2, and BRD4 expression. NMYC plays an important role in the prognosis of patients with neuroblastoma. To assess the effect of GW9662, we evaluated NMYC expression in CHP212 cells after treatment with 0, 5, and 10 μM GW9662 for 5 days. GW9662 treatment significantly decreased NMYC protein expression in a dose-dependent manner (Fig. 3A). Moreover, GW9662 treatment decreased the expression of cell survival-related BCL2 (Fig. 3B). Interestingly, protein expression of BRD4 (Fig. 3C), bromodomain and extraterminal domain (BET) family proteins, and upstream regulators of NMYC (Fig. 3A) and BCL2 (Fig. 3B) was also decreased by GW9662 treatment.

GW9662 treatment induces increased expression of neuronal marker TUBB3. Interestingly, CHP212 cells treated with GW9662 demonstrated remarkable morphological changes, spindle-shaped changes (Fig. 4B). The spindle-shaped changes were confirmed by measuring the circularity $\{4\pi/[\text{area} \times (\text{circumference length})^2]\}$ (Supplemental Fig. 2*). To further explore whether the morphological changes induced by GW9662 treatment reflected cell differentiation, CHP212 cells were stained for the neuronal differentiation associated markers, TUBB3, NFL and NeuroD1. CHP212 cells treated with 5 and 10 μM GW9662 for 7 days showed upregulated NFL, TUBB3 and MAP2 expression, respectively (Fig. 4A, C and Supplemental Fig. 3*). While, NeuroD1, which expression is associated with increased tumorigenesis of neuroblastoma and associated with a poor prognosis, expression level was decreased in a dose dependent manner (Fig. 4C). The dose of GW9662 that induced the expression this marker was almost the same as that which induced the remarkable morphological changes. In contrast, 10 μM 13-cis-RA, a differentiation inducer, was not enough to change CHP212 cell morphology nor increased TUBB3 expression level (Supplemental Fig. 4*).

*See online. https://doi.org/10.3164/jcbn.23-28

doi: 10.3164/jcbn.23-28

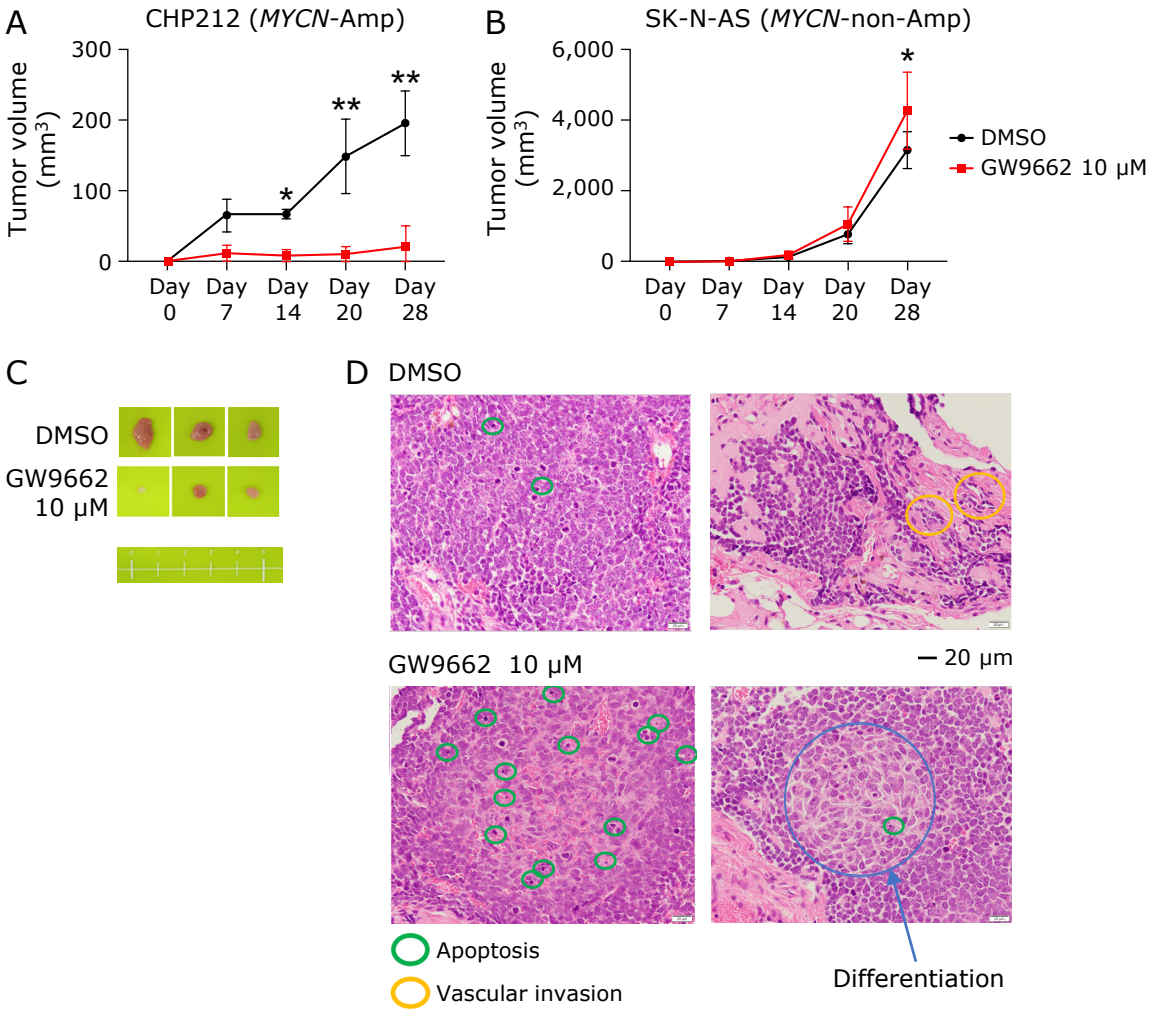

Fig. 5. Effects of GW9662 treatment on tumor histopathology of *MYCN*-amplified or *MYCN*-non-amplified neuroblastoma *in vivo*. CHP212 cells (5×10^6/100 μl matrix gel) or SK-N-AS cells (1.75×10^6/100 μl matrix gel) with or without 10 μM GW9662 in matrix gel, were injected subcutaneously into the back of each mouse. Tumor volume curves of CHP212 xenografts (A) and SK-N-AS xenografts (B) for 4 weeks are shown. Data are presented as the mean ± SE ($n = 4$ or 5). *p<0.05; **p<0.01, relative to non-treated control. P values were calculated using Tukey's multiple comparison test. (C) Representative macroscopic photograph of CHP212 xenograft tumors with (middle panel) or without (upper panel) GW9662 treatment at the end of the experiment. Lower panel shows a ruler, with one scale being 1 cm. (D) Representative histopathology of CHP212 xenograft tumors with (lower panel) or without (upper panel) GW9662 treatment. Note: Apoptotic tumor cells, vascular invasion of tumor cells, and ganglion-like cell differentiation of tumor cells. H & E stain, bars: 20 μm.

GW9662 treatment induced differentiation in *MYCN*-amplified neuroblastoma xenograft mouse models. To evaluate the effects of PPARγ antagonist treatment on the tumor cell differentiation of *MYCN*-amplified and non-amplified neuroblastoma *in vivo*, nude mice were transplanted with *MYCN*-amplified or non-amplified neuroblastoma cells with or without 10 μM GW9662 treatment, and tumor size was measured 4 weeks later. No mice gained or lost more than 10% of their body weight during the observation period.

In the case of *MYCN*-amplified neuroblastoma CHP212 xenografts, tumor growth was remarkably suppressed by 10 μM GW9662 treatment throughout the experimental period (Fig. 5A). In contrast, 10 μM GW9662 treatment did not suppress tumor growth of *MYCN*-non-amplified neuroblastoma SK-N-AS xenografts, but rather increased it compared with the untreated group ($p = 0.0240$) (Fig. 5B). The size of the harvested SK-N-AS xenograft tumors did not show a significant difference between the groups (Supplemental Fig. 5A*).

On the other hand, the size of harvested CHP212 xenograft tumors with GW9662 treatment was remarkably decreased by 85.7% compared with that of DMSO control tumors (p<0.05) (Fig. 5C and Supplemental Fig. 5B*). We excluded the possibility that GW9662 affects cell attachment in the xenograft model. The effect of 10 μM GW9662 treatment on cell attachment was also evaluated. GW9662 treatment did not affect CHP212 cell attachment, as shown in Supplemental Fig. 6*.

Histopathologically, tumor tissues obtained from untreated CHP212 xenograft mice showed a solid growth pattern with a few stromal components (Fig. 5D). Many mitotic cells and vascular invasions were also observed (Fig. 5D). In contrast, many apoptotic tumor cells were observed in the tumor tissues of all CHP212 xenograft mice treated with 10 μM GW9662 (Fig. 5D). Of note, cell differentiation into ganglion-like cells was observed in the tumor tissue treated with 10 μM GW9662 (Fig. 5D).

Discussion

In the present study, we suggested that effects of treatment with a PPAR-γ agonist or antagonist on cell growth in neuro-

*See online. https://doi.org/10.3164/jcbn.23-28

blastoma could be affected by the presence of *MYCN*-amplification. In particular, in our used *MYCN*-amplified neuroblastoma cells, treatment with a PPAR-γ antagonist induced cell differentiation, apoptosis and resultant growth inhibition in a dose-dependent manner, whereas that with a low-to-moderate dose of a PPAR-γ agonist stimulated cell growth.

Our findings that treatment with a PPAR-γ agonist and antagonist affects cell growth of *MYCN*-amplified neuroblastoma are similar to those observed in the previous findings in neural stem/precursor cells treated with PPAR-γ agonists and antagonists.[6,8,19] We realized that one of the similarities between these cells in the report could be explained by the high expression of NMYC, which maintains cell immaturity and survival.[20–22] This observation led to the new hypothesis that treatment with PPAR-γ antagonist may control NMYC expression. As expected, in our study, treatment with a PPAR-γ antagonist significantly decreased NMYC expression in *MYCN*-amplified neuroblastoma. Accordingly, treatment with a PPAR-γ antagonist induced G1 phase arrest, differentiation and apoptosis in *MYCN*-amplified neuroblastoma. Increased ratio of G1 phases could be associated with the differentiation of CHP212 cells in part, because it is well-known that the determination of differentiation is made in G1 phase, and induction of differentiation requires cell-cycle arrest.[23–25] That treatment with a PPAR-γ antagonist suppresses NMYC expression and induces differentiation and apoptosis in *MYCN*-amplified neuroblastoma has not been reported until date. Moreover, the treatment with a PPAR-γ antagonist effectively induced differentiation of CHP212 cells, that is one of the 1p36^{-} neuroblastoma cells and resistant to RA treatment.[26] However, to show the *MYCN*-dependency of the effect of GW9662, we need to use more *MYCN*-non-amplified neuroblastoma cell lines. From clinical view, it is worth to say that we implied alternative medicine for *MYCN*-amplified neuroblastoma, a high-risk tumor of recurrence.[5]

A PPAR-γ antagonist treatment also suppressed expression of the anti-apoptotic protein BCL2. Inhibition of BCL2 effectively suppresses the survival of *MYCN*-amplified neuroblastoma cells.[27] Furthermore, combination therapy using a BCL2 inhibitor and a drug that deregulates NMYC was reported to be effective in killing *MYCN*-amplified tumor cells.[28] Thus, treatment with a PPAR-γ antagonist might result in the induction of differentiation and strong apoptosis in *MYCN*-amplified neuroblastoma through the dual modification of NMYC and BCL2. In addition, we found that expression of BRD4, an upstream regulator of NMYC and BCL2,[29–31] is suppressed by a PPAR-γ antagonist treatment.

In conclusion, a PPAR-γ antagonist suppresses BRD4 protein expression in neuroblastoma and moreover effectively suppresses NMYC and BCL2 expression; this induces differentiation and apoptosis in, probably *MYCN*-amplified, neuroblastoma. Our results suggest a new therapeutic approach focusing not only on cancer features, but also on neuronal features of neuroblastoma, in patients in the high-risk group. We also hope that this study will be helpful for understanding the hitherto unclear mechanisms underlying neuroblastoma.

Author Contributions

YN-I conducted data curation, formal analysis, investigation, visualization and writing–original draft; TN conducted data curation, formal analysis and investigation; SM conducted investigation; TT conducted formal pathological analysis and pathological validation; MW, YS, YI, and MMasuda, YH, TN, and HT performed data curation. GF served as supervisor; MMutoh condected conceptualization, investigation, validation, review & editing and obtained funding.

Acknowledgments

This study was supported grants from Japan Agency for Medical Research and Development (21ck0106556h0002), and supported by the Research Fund of Department of Molecular-Targeting Prevention, Kyoto Prefectural University of Medicine.

Abbreviations

BCL2	B-cell lymphoma 2
BET	bromodomain and extraterminal domain
PPAR	peroxisome proliferator-activated receptor
TUBB3	tubulin beta 3

Conflicts of Interest

No potential conflicts of interest were disclosed.

References

1 Maris JM. Recent advances in neuroblastoma. *N Engl J Med* 2010; **362**: 2202–2211.
2 Matthay KK, Maris JM, Schleiermacher G, *et al*. Neuroblastoma. *Nat Rev Dis Primers* 2016; **2**: 16078.
3 Pinto NR, Applebaum MA, Volchenboum SL, *et al*. Advances in risk classification and treatment strategies for neuroblastoma. *J Clin Oncol* 2015; **33**: 3008–3017.
4 Schnepp RW, Maris JM. Targeting MYCN: a good BET for improving neuroblastoma therapy? *Cancer Discov* 2013; **3**: 255–257.
5 Cole KA, MarisClin JM. New strategies in refractory and recurrent neuroblastoma: translational opportunities to impact patient outcome. *Clin Cancer Res* 2012; **18**: 2423–2428.
6 Nakagawara A, Li Y, Izumi H, Muramori K, Inada H, Nishi M. Neuroblastoma. *Jpn J Clin Oncol* 2018; **48**: 214–241.
7 Ghoochani A, Shabani K, Peymani M, *et al*. The influence of peroxisome proliferator-activated receptor γ_1 during differentiation of mouse embryonic stem cells to neural cells. *Differentiation* 2012; **83**: 60–67.
8 Chiang MC, Cheng YC, Chen HM, Liang YJ, Yen CH. Rosiglitazone promotes neurite outgrowth and mitochondrial function in N2A cells via PPARγ pathway. *Mitochondrion* 2014; **14**: 7–17.
9 Wada K, Nakajima A, Katayama K, *et al*. Peroxisome proliferator-activated receptor γ-mediated regulation of neural stem cell proliferation and differentiation. *J Biol Chem* 2006; **281**: 12673–12681.
10 Culman J, Zhao Y, Gohlke P, Herdegen T. PPAR-γ: therapeutic target for ischemic stroke. *Trends Pharmacol Sci* 2007; **28**: 244–249.
11 Chuang YC, Lin TK, Huang HY, *et al*. Peroxisome proliferator-activated receptors γ/mitochondrial uncoupling protein 2 signaling protects against seizure-induced neuronal cell death in the hippocampus following experimental status epilepticus. *J Neuroinflammation* 2012; **9**: 184.
12 Zolezzi JM, Santos MJ, Bastías-Candia S, Pinto C, Godoy JA, Inestrosa NC. PPARs in the central nervous system: roles in neurodegeneration and neuroinflammation. *Biol Rev Camb Philos Soc* 2017; **92**: 2046–2069.
13 Elrod HA, Sun SY. PPARγ and apoptosis in cancer. *PPAR Res* 2008; **2008**: 704165.
14 Lehrke M, Lazar MA. The many faces of PPARγ. *Cell* 2005; **123**: 993–999.
15 Tachibana K, Yamasaki D, Ishimoto K, Doi T. The role of PPARs in cancer. *PPAR Res* 2008; **2008**: 102737.
16 Vella S, Conaldi PG, Florio T, Pagano A. PPAR gamma in neuroblastoma: the translational perspectives of hypoglycemic drugs. *PPAR Res* 2016; **2016**: 3038164.
17 Lee JJ, Drakaki A, Iiopoulos D, Struhl K. MiR-27b targets PPARγ to inhibit growth, tumor progression and the inflammatory response in neuroblastoma cells. *Oncogene* 2012; **31**: 3818–3825.
18 Ghandi M, Huang FW, Jané-Valbuena J, *et al*. Next-generation characterization of the Cancer Cell Line Encyclopedia. *Nature* 2019; **569**: 503–508.
19 Morales-Garcia JA, Luna-Medina R, Alfaro-Cervello C, *et al*. Peroxisome

doi: 10.3164/jcbn.23-28

proliferator-activated receptor γ ligands regulate neural stem cell proliferation and differentiation *in vitro* and *in vivo*. *Glia* 2011; **59**: 293–307.
20 Nagao M, Campbell K, Burns K, Kuan C-Y, Trumpp A, Nakafuku M. Coordinated control of self-renewal and differentiation of neural stem cells by Myc and the p19ARF-p53 pathway. *J Cell Biol* 2008; **183**: 1243–1257.
21 Sanosaka T, Namihira M, Asano H, *et al*. Identification of genes that restrict astrocyte differentiation of midgestational neural precursor cells. *Neuroscience* 2008; **155**: 780–788.
22 Knoepfler PS, Cheng PF, Eisenman RN. N-myc is essential during neurogenesis for the rapid expansion of progenitor cell populations and the inhibition of neuronal differentiation. *Genes Dev* 2002; **16**: 2699–2712.
23 Marayati R, Bownes LV, Stafman LL, *et al*. 9-cis-UAB30, a novel rexinoid agonist, decreases tumorigenicity and cancer cell stemness of human neuroblastoma patient-derived xenografts. *Transl Oncol* 2021; **14**: 100893.
24 Edlund T, Jessell TM. Progression from extrinsic to intrinsic signaling in cell fate specification: a view from the nervous system. *Cell* 1999; **96**: 211–224.
25 Zhu L, Skoultchi AI. Coordinating cell proliferation and differentiation. *Curr Opin in Genet Dev* 2001; **11**: 91–97.
26 Westerlund I, Shi Y, Toskas K, *et al*. Combined epigenetic and differentiation-based treatment inhibits neuroblastoma tumor growth and links HIF2α to tumor suppression. *Proc Natl Acad Sci U S A* 2017; **114**: E6137–E6146.
27 Ham J, Costa C, Sano R, *et al*. Exploitation of the apoptosis-primed state of MYCN-amplified neuroblastoma to develop a potent and specific targeted therapy combination. *Cancer Cell* 2016; **29**: 159–172.
28 Rickman DS, Schulte JH, Eilers M. The expanding world of N-MYC-driven tumors. *Cancer Discov* 2018; **8**: 150–163.
29 Sundaram S, Mavis C, Gu JJ, Torka P, Hernandez-Ilizaliturri FJ. BRD4 inhibitors enhance the anti-tumor activity of targeted therapy in chronic lymphocytic leukemia. *Blood* 2020; **136 (Suppl 1)**: 37.
30 Lovén J, Hoke HA, Lin CY, *et al*. Selective inhibition of tumor oncogenes by disruption of super-enhancers. *Cell* 2013; **153**: 320–334.
31 Fiskus W, Sharma S, Qi J, *et al*. Highly active combination of BRD4 antagonist and histone deacetylase inhibitor against human acute myelogenous leukemia cells. *Mol Cancer Ther* 2014; **13**: 1142–1154.